Dynamic behaviour of direct spring loaded pressure relief valves in gas service: II reduced order modelling[☆]

C.J. Hős[a], A.R. Champneys[b], K. Paul[c], M. McNeely[c]

[a]*Department of Hydrodynamic Systems, Budapest University of Technology and Economics, 1111 Budapest, Műegyetem rkp. 3. Budapest, Hungary*
[b]*Department of Engineering Mathematics, University of Bristol, Queen's Building Bristol BS8 1TR, UK*
[c]*Pentair Valves and Controls, 3950 Greenbriar Drive, Stafford, TX 77477, USA*

Abstract

A previous study of gas-service direct-spring pressure relief valves connected to a tank via a straight pipe is continued by deriving a reduced-order model for predicting oscillatory instabilities such as valve flutter and chatter. The reduction process uses collocation to take into account a finite number N of acoustic pressure waves within the pipe, resulting in a set of $2N + 3$ ordinary differential equations. Following a novel non-dimensionalization, it is shown analytically that the model can exhibit, at experimentally realistic parameter values, instabilities associated with coupling between the valve and acoustic waves in the pipe. The thresholds for each instability are such that for a given flow rate, the first mode to go unstable as the inlet pipe length increases is the quarter-wave mode, then a three-quarter wave, a 5/4-wave etc. Thus the primary mode of instability should always be due to the quarter wave. In the limit of low flow rates, a simple approximate expression is found for the quarter-wave instability threshold in the form of inlet pipe length against mass flow rate. This threshold curve is found to agree well with simulation of the full model. For higher flow rates there is a need to include fluid convection, inlet pressure loss and pipe friction in order to get good agreement. The reduced model enables the dependence of the stability curve on key dimensionless physical parameters to be readily computed.

Keywords: pressure-relief valve, reduced order modelling, instability, quarter-wave, Hopf bifurcation, acoustic resonance,

[☆]Short title: Reduced order modelling of gas PRVs

Contents

1. Introduction

This paper continues the scientific investigation by the present authors into the mechanisms of instability in direct spring operated pressure relief valves (PRVs), including implications for practical operation. The work follows directly from the results presented by us in Hős et al. (2014). That work showed, for three different industry-standard valve sizes (1E2, 2J3 and 3L4), that when connected to a reservoir via a straight pipe a flutter-type instability is always observed for long enough pipes. A match between experiments and simulation results showed that the instability takes the form of Hopf bifurcation, associated with a a quarter-wave pipe mode. Slightly longer pipes (or equivalently lower mass flow rates) leads to potentially damaging valve chatter, a form of vibro-impact behaviour in which the valve repeatedly impacts with its seat. That paper also contained a comprehensive bibliography on previous published work on pressure-relief valve modelling, to which the reader is referred for a historical introduction to the subject.

One of the weaknesses of the results in Hős et al. (2014) is the lack of a simple design rule for predicting the onset of this instability, other than running a series of computationally expensive gas-dynamic simulations. One way to address this weakness is to make a model reduction, by considering oscillatory acoustic motion only in the quarter-wave. Such a reduction was carried out by Bazsó et al. (2014b), using a collocation method. The reduced-order model so obtained with just a single, quarter-wave mode included was analysed in depth by Bazsó et al. (2014a) for parameter values corresponding to almost incompressible fluid (liquids) and without considering the effects of fluid convection nor pipe friction. There, a rich dynamics was found involving an interplay between a valve-only and a pipe quarter-wave instability.

The results in Bazsó et al. (2014a) are not likely to shed much light on the dynamics of relief valves in gas service though, principally because the dimensionless-parameter that measures the reciprocal of compressibility (called β below) is about five orders of magnitude smaller for the gas-valve configuration considered here, which has a profound effect of the kind of instabilities observed. It is also questionable whether the model developed in Bazsó et al. (2014b) is valid for long pipes, for at least two reasons. First, the treatment of nonlinear effects due to fluid convection, inlet pressure loss and friction effects was incomplete. Previous studies, e.g. by Izuchi (2010) have suggested that pipe friction *may* have a stabilizing influence for long pipes. On the other hand, preliminary simulation results in Bazsó et al.

3

(2014b) suggest that convective terms may have a destabilizing influence. Second, earlier studies by Hayashi (1995) and Botros et al. (1997) suggest that oscillations at frequencies corresponding to higher-order pipe modes can be excited, so more than just a single quarter-wave model may need to be included in the reduced-order model.

The aim of this paper then is to perform a similar model reduction as in Bazsó et al. (2014b), but valid for gas dynamics, and to include an arbitrary number of pipe modes. We The reduced model so-obtained can be further analysed to explain the potential for flutter instabilities and whether friction effects can stabilize the dynamics for very long pipes. Furthermore, by making a careful treatment of the nonlinear terms and performing nondimensionalization, we are able to show how the instability thresholds depend on key physical design parameters, such as the set pressure of the valve, its viscous damping coefficient and the reservoir volume.

The rest of this paper is outlined as follows. First, Sec. 2 presents a reduction of the mathematical model in Hős et al. (2014) by assuming that only a finite number N of pipe modes are excited. Using a collocation method, this results in a set $2N + 3$ nonlinear ordinary differential equations governing the dynamics of the valve, tank pressure and pipe flow. The equations are presented in a fully dimensionless form, amenable to parametric investigation. Sec. 3 then uses these reduced equations to analyse possible coupled valve and pipe mode flutter instabilities that can be observed in this model. It is proved analytically that the instabilities are well ordered, the first mode, a quarter wave, is always the first to go unstable upon increasing the inlet pipe length or decreasing the mass flow rate. This provides *a posteriori* justification for just considering a quarter-wave model. Furthermore an analytical approximation can be found for the instability curve in terms of mass flow rate as a function of pipe length. Sec. 4 considers simulation results of the reduced-order model comparing it to the full model, showing that the two closely agree in predicting the instability. Sec. 5 presents further parameter studies, showing how the onset of pipe flutter depends on various other physical parameters, including those representing the magnitude of pipe friction and fluid convection, as well as various properties of the valve itself. Finally Sec. 6 draws conclusions and suggests implications of the results for pressure relief systems used in practice.

4

Figure 1: Definition sketch of the mathematical model developed in Hős et al. (2014)

2. Model development

In this section we derive a reduced-order model for predicting valve instability, assuming small-amplitude oscillations around an equilibrium lift. In contrast to earlier studies that predict multiple modes of instability in valve-pipe-reservoir systems (e.g. Hayashi (1995) and Botros et al. (1997)) the reduced model will retain nonlinear fluid convection terms and nonlinear pressure-drop inlet effects so that moderate amplitude post-instability motion can still be accurately predicted.

2.1. The full model

The model developed by Hős et al. (2014) considers the system depicted in Fig. 1 consisting of a reservoir, a pipe and a direct spring-loaded valve. The gas properties in the pipe depend both on the axial coordinate ξ along the pipe and time t, hence we have $\rho(\xi, t)$ (density distribution), $p(\xi, t)$ (pressure distribution), $v(\xi, t)$ (gas velocity distribution) and $T(\xi, t)$ (temperature distribution) with $\xi = 0$ being the reservoir-end of the pipe and $\xi = L$ being the valve-end of the pipe. Standard rigid-body and gas dynamic assumptions lead to the following system of differential equations for the valve lift $x_v(t)$ and reservoir pressure $p_r(t)$, respectively:

$$m\ddot{x}_v + k\dot{x}_v + s(x_p + x_v) = (p_v - p_b)A_{\text{eff}}(x_v) \qquad \text{for } x_v > 0, \qquad (1)$$

5

$$\dot{p}_r = \frac{a^2}{V}\left(\dot{m}_{\text{in}} - \dot{m}_{\text{out}}\right), \tag{2}$$

where $\dot{m}_{\text{in}}$ is the *constant* flow rate entering the reservoir, $\dot{m}_{\text{out}}$ is the mass flow rate entering the pipe from the reservoir: $\dot{m}_{\text{out}} = \rho(0,t)A_{\text{pipe}}v(0,t)$, $p_v = p(L,t)$ is the valve-end pressure and p_b stands for the back pressure. We shall note here that although this formulation allows any time-dependent inlet mass flow rate $\dot{m}_{\text{in}}$, we confine ourselves to the case when it is constant.

The so-called set pressure p_{set} is the pressure at which the valve pops open, i.e. $sx_p = (p_{\text{set}} - p_0)A_{\text{eff}}(0)$. The function $A_{\text{eff}}(x_v)$ was introduced in Hős et al. (2014) as the *effective area* of the valve. By definition, A_{eff} is the fluid force on the valve divided by the (static) pressure difference $p_v - p_b$ and enables us to conveniently combine the pressure and fluid momentum effects on the valve into a single expression. Note that for a commercial valve the shape of A_{eff} determines key properties of the valve behaviour such as the valve lift at a given pressure and the the pressure value, typically a few percent lower than p_{set}, at which the valve is designed to close (the so-called *blow-down pressure*). Since our goal is not a detailed experimental matching in this paper, nor to look at the transient effects caused by valve opening or closing, for simplicity we shall assume the effective area function to be

$$A_{\text{eff}} = \begin{cases} \frac{\pi}{4}D_{\text{eff}}^2 & \text{if } x_v > 0 \quad \text{and} \\[2mm] \frac{\pi}{4}D_{\text{seat}}^2 & \text{if } x_v = 0, \end{cases} \tag{3}$$

where D_{eff} is the effective diameter of the lift area of the valve when it is open. Moreover, as it was demonstrated in Hős et al. (2014) and will be explained analytically in section 3 below, the shape of the effective area curve is not the root cause of valve flutter instabilities. We have therefore assumed the simplified form (3) throughout the rest of this study to produce minimalist models capable of explaining the onset of flutter and chatter. The results are easily extendable to include more realistic effective area curves.

During valve oscillations and especially valve chatter, the valve might hit the seat ($x_v = 0$) or the upper stopper ($x_v = x_{max}$), for which the impact law is given by

$$\dot{x}_v^+ = -r\dot{x}_v^-, \tag{4}$$

meaning that the velocity of the valve immediately after the impact $\dot{x}_v^+$ is less than the velocity before the impact $\dot{x}_v^-$ ($0 \leq r \leq 1$) and the direction reverses.

The dynamics of the pipe gas flow is governed by the standard 1D unsteady equation of continuity, equation and motion and energy equation (see Zucker and Biblarz (2002) for details):

$$\frac{\partial \mathcal{U}}{\partial t} + \frac{\partial \mathcal{F}}{\partial \xi} = \mathcal{Q}, \tag{5}$$

with

$$\mathcal{U} = \begin{pmatrix} \rho \\ \rho v \\ \rho e \end{pmatrix}, \quad \mathcal{F} = \begin{pmatrix} \rho v \\ \rho v^2 + p \\ \rho e v + p v \end{pmatrix} \quad \text{and} \quad \mathcal{Q} = \begin{pmatrix} 0 \\ \rho f \frac{v|v|}{2 D_{\text{pipe}}} \\ 0 \end{pmatrix}, \tag{6}$$

with f being the friction factor of the pipe. Here $\rho(\xi,t)$, $v(\xi,t)$, $p(\xi,t)$ and $e(\xi,t)$ are density, velocity, pressure and internal energy distribution along the pipe axis $0 \leq \xi \leq L$ that might vary in time t.

The inflow from the reservoir into the pipe is assumed to be ideal, hence the total enthalpy remains constant:

$$h_r(t) = c_p T_r(t) = c_p T(0,t) + \frac{1}{2}\left(v(0,t)\right)^2. \tag{7}$$

At the valve-end of the pipe, we require the mass flow rate leaving the pipe to be equal to the instantaneous mass flow rate through the valve:

$$\rho(L,t) A_{\text{pipe}} v(L,t) = c_2 x_v \sqrt{\rho(L,t)\, p(L,t)}. \tag{8}$$

Here, the term of the right-hand side is the *choked* mass flow rate leaving the pipe through the valve and

$$c_2 = C_d D_{\text{ft}} \pi \sqrt{\hat{\gamma}\left(\frac{2}{\hat{\gamma}+1}\right)^{\frac{\hat{\gamma}+1}{\hat{\gamma}-1}}}, \tag{9}$$

where C_d is the discharge coefficient (assumed to be constant in this study), $\hat{\gamma} = c_p/c_v$ is the ratio of heat capacities and $D_{\text{ft}} \pi x_v$ is the flow-through area. In typical industrial of such valves (in gas service) the upstream pressure level ensures the choked flow conditions at the valve outlet.

In addition, the sonic velocity in the reservoir $a^2 = \hat{\gamma} R T_r$ in equation (2) is considered to be constant due to the constant reservoir temperature. Also, we assume that the downstream pressure p_b in (1) (also referred to as backpressure) is constant and equal to ambient pressure p_0.

Quantity	Symbol	Value	Units
Mass flow rate	$\dot{m}_{r,in}$	0-16.9	$\mathrm{lb_m/s}$
Capacity mass flow rate	$\dot{m}_{\mathrm{cap}}$	16.9	$\mathrm{lb_m/s}$
Pipe length	L	0-36	inch
Pipe diameter (nom. inner)	D_{pipe}	2.067	inch
Effective pressure diameter	D_{eff}	1.976	inch
Seat diameter	D_{seat}	1.604	inch
Bore diameter	D_{ft}	1.363	inch
Reservoir volume	V	375	$\mathrm{ft^3}$
Total effective moving mass	m	3.18	$\mathrm{lb_m}$
Spring constant	s	714	$\mathrm{lb_s/inch}$
Damping coefficient	% of k_{crit}	0%	$\mathrm{lb_s\,s/inch}$
Set pressure	p_{set}	250	psi
Spring pre-compression	x_p	0.7078	inch
Coefficient of discharge	C_d	0.93	-
Coefficient of restitution	r	0.8	-
Maximum lift	x_{max}	0.472	inch
Ambient temperature	T_0	293	K
Ambient pressure	p_0	14.7	psi
Gas constant	R	288	J/(kgK)
Specific heat ratio	$\hat{\gamma}$	1.4	-
Friction factor	f	0.02	-

Table 1: Physical parameter values of the selected 2J3 valve.

Table 1 gives a definition of all the physical constants used in the equations, together with the values used in this study. These parameter values correspond to those of the middle-size valve tested in Hős et al. (2014), namely a 2J3, for which good agreement was found between experiment and simulation.

2.2. Simplification and non-dimensionalization

We shall now introduce an enhanced non-dimensionalization of this model than was presented in Hős et al. (2014), and make clearer the assumptions that we make in so doing. Suppose that the pipe is long enough to assume that the heat loss through the pipe wall is sufficiently rapid for temperature to be treated as approximately constant. This assumption means that one

does not need to solve the energy equation, i.e. the third component of (6). Moreover, assume that the density ρ of the gas depends only on pressure p (that is the fluid is *barotropic*) so that the *sonic velocity* a can be defined via

$$\frac{1}{a^2} = \frac{\mathrm{d}\rho(p)}{\mathrm{d}p}.$$

We shall analyze the equations of motion for a given mass flow rate $\dot{m}_{r,in}$ close to an assumed valve-open steady-flow equilibrium given by $x = x_e$, $p_r = p_{r,e}$, $T = T_{r,e}$, $\rho = \rho_e$ and sonic velocity $a = a_e$ within the tank. Then, the equation of continuity – the first component of (6) – can be written as

$$0 = \frac{\partial \rho}{\partial t} + \frac{\partial \rho v}{\partial \xi} = \frac{\mathrm{d}\rho}{\mathrm{d}p}\frac{\partial p}{\partial t} + \rho_e \frac{\partial v}{\partial \xi} + v\frac{\mathrm{d}\rho}{\mathrm{d}p}\frac{\partial p}{\partial \xi} = \frac{1}{a_e^2}\left(\frac{\partial p}{\partial t} + \rho_e a_e^2 \frac{\partial v}{\partial \xi} + v\frac{\partial p}{\partial \xi}\right). \tag{10}$$

Here, we have assumed that ρ_e is a constant. This is a reasonable approximation, because we shall only be considering dynamics at pressures that are a moderate perturbation from p_{set}.

Similar manipulation of the momentum equation, the second component of (6), gives

$$0 = \frac{\partial v}{\partial t} + v\frac{\partial v}{\partial \xi} + \frac{1}{\rho_e}\frac{\partial p}{\partial \xi} - \frac{f}{2D}v|v|. \tag{11}$$

Let us introduce a reference frequency ω to be the valve-spring natural frequency and a reference length x_{ref} as

$$\omega^2 = \frac{s}{m} \quad \text{and} \quad x_{\text{ref}} = A_{\text{eff}}(0)\frac{p_0}{s}.$$

We then define dimensionless pressure, spatial, temporal and velocity variables via

$$p = p_0\,\tilde{p}, \quad \xi = L\,\zeta, \quad t = \frac{\tau}{\omega} \quad \text{and} \quad v = x_{\text{ref}}\,\omega\,\tilde{v}.$$

We also introduce three more dimensionless dynamic variables y_{1-3} for the valve lift, valve velocity and reservoir pressure, defined via

$$x = x_{\text{ref}}\,y_1, \quad v = x_{\text{ref}}\,\omega\,y_2, \quad \text{and} \quad p_r = p_0\,y_3.$$

It is useful to non-dimensionlize mass flow rate with respect to the valve's *capacity* flow rate $\dot{m}_{\text{cap}}$, the rated maximum mass flow rate through the valve.

This is defined as the flow which corresponds to a tank pressure 10% above set pressure p_{set} and at $x_v = x_{\text{max}}$, the upper stopper of the valve lift. That is,

$$\dot{m}_{\text{cap}} = c_2 x_{max} \sqrt{\rho_e (1.1 \times p_{\text{set}})}\,, \tag{12}$$

with c_2 defined by (9).

After these re-scalings, the valve and reservoir dynamics become

$$y_1' = y_2, \tag{13}$$
$$y_2' = (\tilde{p}(1, \tau) - 1) - \kappa y_2 - (\delta + y_1), \tag{14}$$
$$y_3' = \beta \left(q - \mu \tilde{v}(0, \tau) \right), \tag{15}$$

where a prime ($'$) denotes $\frac{d}{d\tau}$, $\tilde{p}(1, \tau)$ is the dimensionless pressure at the valve-end of the pipe ($\xi = L$) and $\tilde{v}(0, \tau)$ is the dimensionless velocity at the reservoir-end of the pipe ($\xi = 0$). Here κ is the dimensionless viscous damping on the valve, δ is the dimensionless spring precompression. The parameter β measures the compressibility of the system; for gas service systems β is several orders of magnitude smaller than for liquid service systems. Note that q measures the inlet mass flow rate as a fraction of the valve capacity; that is, $q = 1$ means $\dot{m}_{\text{in}} = \dot{m}_{\text{cap}}$. The multiplier μ arising during the nondimensionalization represents a ratio of two mass flow rates

$$\mu = \frac{A_{\text{pipe}} \rho_e \omega x_{\text{ref}}}{\dot{m}_{\text{cap}}}. \tag{16}$$

The precise definition and the actual values of these dimensionless parameters, along with some additional ones yet to be defined, are given in Table 2, based on the data in Table 1.

After a similar rescaling process the fluid dynamic equations (10) and (11) can be rewritten as

$$0 = \frac{\partial \tilde{p}}{\partial \tau} + \frac{\alpha}{\gamma} \frac{\partial \tilde{v}}{\partial \zeta} + \Lambda \tilde{v} \frac{\partial \tilde{p}}{\partial \zeta} \quad \text{and} \tag{17}$$

$$0 = \frac{\partial \tilde{v}}{\partial \tau} + \Lambda \tilde{v} \frac{\partial \tilde{v}}{\partial \zeta} + \frac{1}{\alpha \gamma} \frac{\partial \tilde{p}}{\partial \zeta} - \phi \tilde{v} |\tilde{v}|. \tag{18}$$

Here

$$\Lambda = \frac{x_{\text{ref}}}{L} = \frac{A p_0}{sL} = \frac{\nu \alpha}{\gamma} \tag{19}$$

10

Quantity	Symbol	Definition	Value
Reference pressure	p_{ref}	$p_b = p_0$	14.7 psi
Reference displacement	x_{ref}	$\frac{A_{\mathrm{eff}} p_{\mathrm{ref}}}{s}$	0.0623 inch
Reference frequency	ω	$\sqrt{s/m}$	294.6 rad/s
Reference velocity	v_{ref}	$x_{\mathrm{ref}}\omega$	18.35 inchs^{-1}
Capacity mass flow rate	$\dot{m}_{\mathrm{cap}}$	eq. (12)	16.86 $\mathrm{lb_m}/s$
Mass flow rate ratio	μ	eq. (16)	0.00209059
Driving mass flow rate	q	$\frac{\dot{m}_{\mathrm{in}}}{\dot{m}_{\mathrm{cap}}}$	varied
Spring pre-compression	δ	$\frac{s x_p}{A_{\mathrm{seat}} p_b}$	11.3607
Pipe length parameter	γ	$\frac{L\omega}{a}$	varied
Reservoir-size parameter	β	$\frac{a_e^2}{V}\frac{\dot{m}_{\mathrm{cap}}}{p_{\mathrm{ref}}\omega}$	0.029
Valve Damping	κ	$\kappa = \frac{k}{m}\sqrt{\frac{m}{s}}$	0
Velocity-to-mass flow rate par.	σ	eq. (24)	12.199
Ambient pressure	ν	$\frac{p_0}{\rho_e a_e^2}$	0.0532
Velocity-to-sonic velocity par.	α	$\frac{\rho_e A_{\mathrm{eff}} a_e}{m\omega} = \frac{1}{\nu}\frac{v_{\mathrm{ref}}}{a_e}$	0.0255
Friction factor	ϕ	$f\frac{x_{\mathrm{ref}}}{2 D_{\mathrm{pipe}}}$	0.000344
Inlet pressure drop par.	χ	eq. (23)	1.72×10^{-5}
Coefficient of restitution	r	r	0.8

Table 2: Reference scales and dimensionless parameters together with their values for the data in Table 1.

is the ratio of the valve length scale to the pipe length. Note that

$$\gamma = L\omega/a = \frac{1}{2}\frac{2L}{a}2\pi f_{\text{valve}} = \pi f_{\text{valve}}/f_{\text{pipe}} \tag{20}$$

is the ratio of the valve and pipe eigenfrequencies, and is such that we have resonance between the pipe and the valve if $\gamma = \pi$.

2.3. Model reduction

We now perform a model reduction by assuming that, upon ordering the acoustic pipe modes by their wavenumber (number of full wavelengths within the pipe), only the first N waves are excited. Note that waves of higher wavenumber have a higher frequency, and as can easily be seen in the analysis in Sec. 3 below, are excited at higher mass flow rates. Hence our approximation is consistent with the assumption of small-amplitude oscillatory behaviour because energy will likely be in lower frequency waves that are closer to their instability threshold.

The derivation follows closely that in Bazsó et al. (2014b) where a reduced-order model for a valve in liquid service was derived, assuming that the first, quarter-wave mode dominates the pipeline dynamics. The present derivation is in principle much more general as it allows for an arbitrary number N of modes and shall involve other subtleties including a non-dimensionalization that enables the relationship between the instabilities associated with each mode to become apparent. Moreover, we shall additionally include the effect of pipe inlet pressure drop. That is, the drop in pressure as the gas accelerates from the reservoir to the pipe ideally, which results in different reservoir and pipe inlet pressure (as well as temperature and density). It was found that inclusion of this effect was necessary to get close quantitative match with the full model.

Specifically, we restrict the pipe model (17) and (18) to the usual sinusoidal "organ pipe" modes that fit the boundary conditions (7), (8). First, we decompose the pressure and velocity distribution in the pipe as

$$\tilde{p}(\tau,\zeta) = y_3(\tau) - \chi\left(\tilde{v}(0,\tau)\right)^2 + \sum_{k=1}^{N} B_k(\tau)\sin\left(2\pi\frac{\zeta}{4}(2k-1)\right) \tag{21}$$

$$\tilde{v}(\tau,\zeta) = \sigma y_1\sqrt{\tilde{p}(1,\tau)} + \sum_{k=1}^{N} C_k(\tau)\cos\left(2\pi\frac{\zeta}{4}(2k-1)\right). \tag{22}$$

Here $B_k(t)$ and $C_k(t)$, $k = 1, \ldots, N$ are *a priori* unknown wave amplitudes that need to be solved for and the new parameters are

$$\chi = \frac{\rho_e x_{\text{ref}}^2 \omega_v^2}{2 p_{\text{ref}}} \tag{23}$$

and

$$\sigma = \frac{c_2 x_{\text{ref}} \sqrt{\rho_e p_{\text{ref}}}}{A_{\text{pipe}} \rho_e x_{\text{ref}} \omega_v}. \tag{24}$$

The above expressions ensure that the boundary conditions are fulfilled because

$$\tilde{p}(0, \tau) = y_3(\tau) - \chi \left(\tilde{v}(0, \tau) \right)^2$$

and

$$\tilde{v}(1, \tau) = \sigma y_1 \sqrt{\tilde{p}(1, \tau)}.$$

Note also that to fit these conditions, only waves with wavelengths $4L$, $4L/3$, $4L/5$, … are selected, as is usual for a pipe that is open at one end (the reservoir end) and closed at the other (the valve end).

At this point, (21) and (22) define the pressure and velocity distribution only implicitly because we need an expression for $(\tilde{v}(0, \tau))^2$ and $\sqrt{\tilde{p}(1, \tau)}$. Hence we evaluate $\tilde{v}(0, \tau)$ in (22), substitute it into (21), evaluate it at $\xi = 1$ and obtain

$$0 = \left(1 + \chi \sigma^2 y_1^2 \right) \tilde{p}(1, \tau) + 2 \chi \sigma y_1 \left(\sum_k C_k \right) \sqrt{\tilde{p}(1, \tau)} - y_3 + \chi \left(\sum_k C_k \right)^2 - \sum_{k=1}^{N} (-1)^{k+1} B_k, \tag{25}$$

which now needs to be solved for $\sqrt{\tilde{p}(1, \tau)}$. As already stressed, we are searching for a model that is valid close to the valve equilibrium, that is for small B_k and C_k values. Therefore we can expand the solution of equation (25) as a Taylor series around $C_k = B_k = 0$ to obtain

$$\sqrt{\tilde{p}(\tau, 1)} \approx \sqrt{\frac{y_3}{Z}} \left(1 + \frac{\sum_{k=1}^{N} (-1)^{k+1} B_k}{2 y_3} \right) + \frac{Z - 1}{Z} \frac{1}{\sigma y_1} \sum_{k=1}^{N} C_k + \mathcal{O}(2), \tag{26}$$

where $\mathcal{O}(2)$ refers to terms that are second order or higher in coefficients B_k and C_k for $k = 1, \ldots, N$ and we have used the abbreviation

$$Z(y_1, \chi) = 1 + \chi y_1^2 \sigma^2 .$$

13

Similar manipulation gives

$$(\tilde{v}(\tau,0))^2 \approx \frac{v_O^2}{Z}\left(1 + \frac{\sum_{k=1}^{N}(-1)^{k+1}B_k}{y_3}\right) + \frac{2}{Z^{3/2}}v_O\sum_{k=1}^{N}C_k + \mathcal{O}(2). \quad (27)$$

where $v_O = \sigma y_1\sqrt{y_3}$ represents the dimensionless orifice flow through the valve at equilibrium, ignoring inlet pressure drop and friction effects. Finally, expressions (26) and (27) truncated at first-order are substituted back into (21) and (22).

Next, we substitute (21) and (22) into the continuity equation (17) and equation of motion (18) of the fluid in the pipe. To close the system we use the well-know method of collocation (see e.g. Canuto et al. (2007)). That is, we prescribe that the equations (17) and (18) are exactly fulfilled at evenly spaced grid points

$$\zeta = \zeta_k = \frac{k}{N+1}, \quad \text{with} \quad k = 1,2\ldots N.$$

These prescriptions lead to algebraic equations that link the wave-mode amplitudes B_k and C_k, $k = 1, 2, \ldots N$, to their corresponding first order time derivatives, B_k' and C_k'.

Upon carrying out this substitution and evaluation, we obtain the $2N$-dimensional system of first-order ordinary differential equations

$$B_k' = -a_k y_3' + b_k\frac{\alpha}{\gamma}C_k$$

$$+ \Lambda\left(v_O\sum_m \tilde{b}_{km}B_m + \sum_{m,n}\hat{b}_{kmn}B_mC_n + \frac{v_O}{y_3}\sum_{m,n}\bar{b}_{kmn}B_mB_n\right)$$

$$+ \mathcal{O}(\chi), \qquad (28)$$

$$C_k' = (-1)^k a_k\frac{d}{d\tau}\hat{V}_1 - b_kB_k\frac{1}{\alpha\gamma} +$$

$$+ \Lambda\left(v_O\sum_m \tilde{c}_{km}C_m + \frac{v_O}{y_3}\sum_{m,n}\hat{c}_{kmn}B_mC_n + \sum_{m,n}\bar{c}_{kmn}C_mC_n\right)$$

$$+ \phi\left(f_kv_O^2 + 2v_OC_k + \hat{f}_kC_k^2 + \sum_m \tilde{f}_{km}\frac{v_O^2}{y_3}B_m + \sum_{m,n}\bar{f}_{kmn}\frac{v_O^2}{y_3^2}B_mB_n\right)$$

$$+ \mathcal{O}(\chi), \qquad (29)$$

	$k = 1$	$k = 2$	$k = 3$	$k = 4$	$k = 5$
a_1	1.4142				
a_2	1.1547	0.4227			
a_3	1.3066	0.3244	0.2168		
a_4	1.2311	0.4242	0.1682	0.1336	
a_5	1.2869	0.3804	0.2392	0.1059	0.091

Table 3: Linear coefficients a_k for $N = 1 \ldots 5$

The form of the $\mathcal{O}(\chi)$ terms can be written out explicitly. However this leads to formulae that are extremely cumbersome and would run over several pages. We omit the details here for brevity. Nevertheless, the form of these equations for any N is clear. Each pair of equations for the B_k and C_k consists of four parts: a linear part with coefficients a_k and b_k and three additional, nonlinear parts taking into account the convection terms (parameter Λ), the pipe friction (parameter ϕ) and the inlet pressure drop (parameter χ).

The actual values of the coefficient b_k is given explicitly by

$$b_k = (2k - 1)\pi/2$$

and does not change as the total number of modes N is varied (provided of course that $N > k$), whereas in general all other coefficients a_k, $\tilde{b}_{km}$, etc. do vary slightly with the choice of N; see Table 3 for the case of the other linear coefficient a_k. This is because the collocations points $\zeta_k = L\frac{k}{N+1}$ vary with N. Nevertheless, standard mathematical theorems show that the collocation method converges as $N \to \infty$ (in the sense that the residual decays uniformly to zero). The values of all the coefficients for each k and N can easily be found numerically using computer algebra.

Finally, the above system of ordinary differential equations is coupled with the valve and reservoir dynamics described by (13)-(15) via evaluation of $\tilde{p}(1, \tau)$ and $\tilde{v}(0, \tau)$ up to linear terms in the C_k and B_k. Specifically, from (26) and (27), we obtain

$$\tilde{p}(\tau, 1) \approx \hat{P}_1 := \frac{y_3}{Z}\left(1 + \frac{\sum_{k=1}^{N}(-1)^{k+1}B_k}{y_3}\right) + \frac{2\sqrt{y_3}}{\sigma y_1}\frac{Z-1}{Z^{3/2}}\sum_{k=1}^{N}C_k, \quad (30)$$

$$\tilde{v}(\tau, 0) \approx \hat{V}_0 := \frac{v_O}{\sqrt{Z}}\left(1 + \frac{\sum_{k=1}^{N}(-1)^{k+1}B_k}{2y_3}\right) + \frac{\sum_{k=1}^{N}C_k}{Z}, \quad (31)$$

$$\tilde{v}(\tau, 1) \approx \hat{V}_1 := \frac{v_O}{\sqrt{Z}}\left(1 + \frac{\sum_{k=1}^{N}(-1)^{k+1}B_k}{2y_3}\right) \quad (32)$$

$$(33)$$

The coefficients for the one-mode model (including only the quarter-wave mode) can be calculated explicitly, to give the equations

$$y_1' = y_2$$
$$y_2' = (\hat{P}_1 - 1) - \kappa y_2 - (\delta + y_1),$$
$$y_3' = \beta\left(q - \mu\hat{V}_0\right), \quad (34)$$
$$B_1' = -\sqrt{2}y_3' + \frac{\pi\alpha}{2\gamma}C_1 - \Lambda\frac{\pi}{2}B_1\left(\hat{V}_1 + \frac{C_1}{\sqrt{2}}\right), \quad (35)$$
$$C_1' = -\sqrt{2}\frac{d}{d\tau}\hat{V}_1 - \frac{\pi}{2\alpha\gamma}B_1 + \Lambda\frac{\pi}{2}C_1\left(\hat{V}_1 + \frac{C_1}{\sqrt{2}}\right) + \phi\left(\sqrt{2}\hat{V}_1^2 + 2\hat{V}_1C_1 + \frac{1}{\sqrt{2}}C_1^2\right).$$

where $\hat{P}_1(y_1, y_3, B, C; \chi)$ and $\hat{V}_0(y_1, y_3, B, C; \chi)$ are given by expressions (30) and (31) with $N = 1$ and $\hat{V}_1 = \sigma y_1\sqrt{\hat{P}_1}$ is the dimensionless flow velocity at the valve-end of the pipe. Note that the in the above system, B_1' is only implicitly defined because taking $\frac{d}{d\tau}\hat{V}_1$ means further terms B_1' appear on the right-hand side. Finally, we also note that the above form agrees with the result in Bazsó et al. (2014b) for the case $\chi = 0$, up to quadratic approximation.

3. Qualitative instability analysis

In Hős et al. (2014) we found evidence for two kinds of instability phenomena; an oscillatory instability causing pipe flutter (in the language of dynamical systems, a Hopf bifurcation) and a static jump in the valve lift for a continuous change in conditions (a fold bifurcation). The latter we

16

Pipe length L [inch]	valve f_v [Hz]	1/4 pipe f_1 [Hz]	3/4 pipe f_2 [Hz]	5/4 pipe f_3 [Hz]
12	73.6	281	844	1207
36	73.6	93.8	281	470
72	73.6	47	141	234

Table 4: Important system frequencies for different pipe lengths, in dimensional units given other parameter values as in Table 1. The pipe-mode frequencies are given by $f_k = a/\lambda_k$ with a being the sonic velocities and $\lambda_k = \frac{4L}{2k-1}$ the wavelength.

showed was caused by a non non-trivial effective-area versus lift relationship $A_{\text{eff}}(x_v)$ and does not lead to flutter or chatter. These jumps do not lead to instabilities themselves, but can be contributory factors in any practical implementation because they can cause a valve to jump into or out of a mass flow rate that corresponds to instability. In contrast, the Hopf bifurcation causes a transition to valve flutter which quickly becomes chatter under further decrease of mass flow rate. Moreover we showed that the Hopf bifurcation was always associated with the first acoustic mode in the pipe, whose wave length is $4L$. Here we shall use the reduced-order model (13)–(15), (28), (29) to analyse the precise conditions under which this bifurcation occurs, as well as those corresponding to higher-order pipe modes.

3.1. Pipe-mode instabilities

In what follows we shall assume that the valve is open, the reservoir inlet mass flow rate q is constant and that $A_{\text{eff}} = (\pi/4)D_{\text{eff}}^2$ is a constant. We wish to analyze the stability of the balanced equilibrium state to the reduced system of equations (13)–(15), (28), (29) in which the valve is at its equilibrium state for that flow rate and there are no excited waves in the pipe. For simplicity, we shall ignore the effects of friction, and convection $\phi = \Lambda = 0$ in (28) and (29). The analysis can easily be extended to include these terms, but this leads to extremely cumbersome formulae with little additional insight. Under this assumption we we can look for an equilibrium in which

$$y_1 = x_0, \quad y_2 = 0, \quad y_3 = P_0, \quad B_k = C_k = 0, \text{ for } k = 1, \dots N, \qquad (36)$$

where

$$P_0 = \frac{q^2}{(\mu \sigma x_0 (1 + \chi \sigma^2 x_0^2))^2}, \qquad (37)$$

17

and x_0 solves the polynomial equation

$$(1 + \chi\sigma^2 x_0^2)^2[x_0^3 + (\delta + 1)x_0^2] - \left(\frac{q}{\mu\sigma}\right)^2 = 0. \tag{38}$$

Note that provided $\chi\sigma^2$ is sufficiently small this equation must have a unique positive solution.

Natural frequencies are given in Table 4. Rather than look for resonances between pipe and valve, it is instructive to consider situations in which the valve motion and pipe oscillation and fully coupled and to seek conditions under which the valve effectively applies negative damping to a pipe mode. We consider small perturbations to the equilibrium

$$y_1 = x_0 + \varepsilon Y(t), \quad y_2 = 0, \quad y_3 = P_0 + \varepsilon P(t),$$
$$B_i = C_i = 0, \text{ for } i \neq k, \quad B_k, C_k = \mathcal{O}(\varepsilon), \tag{39}$$

where $\varepsilon > 0$ is a small parameter. Consider again equation (35). Differentiating the forth component (B_k'), making use of the fifth component (C_k') and upon substituting (39) to first order in ε we obtain

$$B_k'' + \left(\frac{b_k}{\gamma}\right)^2 B_k = a_k\beta\mu\sigma\frac{d}{d\tau}\hat{V}_0 + (-1)^k a_k b_k \frac{\alpha}{\gamma}\frac{d}{d\tau}\hat{V}_1$$

$$= (-1)^k a_k b_k \frac{\alpha}{\gamma}\sigma\frac{d}{d\tau}\left(Y\sqrt{P_0} + \frac{x_0}{\sqrt{P_0}}(-1)^{k+1}B_k\right) + \mathcal{O}(\beta), \tag{40}$$

where we have used that $\frac{dy_3}{d\tau} \propto \beta$ from (15) and that $\beta \ll 1$ for a highly compressible fluid (see its value in Table 2). Hence to leading order in β, we can suppose that the reservoir is large enough to keep an approximately constant pressure, i.e. $\frac{dy_3}{d\tau} = \frac{dP}{d\tau} = 0$, so that $y_3 = P_0 + P = \text{const}$. Hence the reservoir pressure variation is negligible ($P = 0$) and is assumed to be equal to its equilibrium pressure P_0.

Suppose that we seek an instability in which the kth pipe mode is excited. Then coupling the valve dynamics to the modal equation for B_k and C_k, and after substitution of (39) with $P(t) = 0$ into (13), (14), we obtain

$$Y'' = -Y + (-1)^{k+1}B_k - \kappa Y' \tag{41}$$

$$B_k'' = -\omega_k^2 B_k + (-1)^k K_k \left(\sqrt{P^0}\, Y' + (-1)^{k+1}\frac{x_0}{2\sqrt{P_0}}B_k'\right), \tag{42}$$

18

where ω_k is the kth pipe eigenfrequency

$$\omega_k = \frac{(2k-1)\pi}{2\gamma} \tag{43}$$

and

$$K_k = a_k b_k \frac{\alpha}{\gamma} \sigma.$$

We can identify the term multiplying K_k in (42) as a kind of damping term. We are looking for a transition point at which this damping term goes from negative to positive (which is precisely the condition for a Hopf bifurcation to occur, see e.g. Kuznetsov (2004)). Hence we can look for a regime in which this K_k term is $O(\varepsilon)$ smaller than the first term on the right-hand side of (42). We can then use multiple timescale asymptotic analysis where the slow time is $O(\varepsilon)$. Specifically, we look for a solution to (41) in the form

$$B_k(\tau; \tau_2) = A(\tau_2) \cos(\omega_k \tau)$$

where $\tau_2 = \varepsilon t$. Substitution of this form into equation (41) gives

$$y'' + \kappa y' + y = (-1)^{k+1} A(\tau_2) \cos(\omega_k \tau),$$

which has forced response solution (after transients have decayed)

$$y(\tau) = (-1)^k \frac{A(\tau_2)}{\omega_k^2 - 1} \cos(\omega_k \tau) + \mathcal{O}(\kappa) = \frac{(-1)^k}{1 - \omega_k^2} B_k + \mathcal{O}(\kappa). \tag{44}$$

We shall also assume that the valve damping κ is similarly week $\mathcal{O}(\varepsilon)$ (actually in our simulations we take $\kappa = 0$, but see from Fig. 7 in Sec. 5 below that 1% or 10% valve damping makes negligible difference), and so we shall drop the $\mathcal{O}(\kappa)$ term as being asymptotically smaller than the $\mathcal{O}(1)$ terms. Then, re-substitution of (44) back into equation (42) gives that the damping term is

$$(-1)^k K_k (-1)^{k+1} \left(\frac{x_0}{2\sqrt{P_0}} - \frac{\sqrt{P_0}}{\omega_k^2 - 1} \right) B_k'$$

$$= - K_k \left(\frac{x_0}{2\sqrt{P_0}} - \frac{\sqrt{P_0}}{\omega_k^2 - 1} \right) B_k'.$$

19

Now, provided that the term in round brackets is positive, this provides positive damping, if it is negative, we get growing oscillations (negative damping). Hence our condition for stability is that

$$\frac{\sqrt{P_0}}{\omega_k^2 - 1} \leq \frac{x_0}{2\sqrt{P_0}}$$

which can be rearranged to give

$$x_0 \geq 2\frac{P^0}{\omega_k^2 - 1}, \tag{45}$$

with a (kth-mode) Hopf bifurcation occurring when we have equality in this expression.

Note from the form of the equilibrium (37) conditions that the condition (45) can be rewritten in the form

$$(1 + \chi\sigma^2 x_0^2)^2(x_0)^3 \geq 2\frac{q^2}{\mu^2\sigma^2(\omega_k^2 - 1)}, \tag{46}$$

that is, stability is achieved if the valve lift is high enough. Note also from (38) that, provided $\chi\sigma^2 \ll 1$, for small q the lift $x_0 \sim \mathcal{O}(q)$ (see also (47) below). Hence for sufficiently small q the inequality (46) will be violated and we will get instability. In contrast, since ω_k given by (43) is proportional to the reciprocal of the dimensionless pipe length γ, the right-hand side of (46) tends to zero as the pipe length L tends to zero. Thus, for each pipe mode k, for a fixed flow rate q we should expect stability for sufficiently short pipes.

3.2. The ordering of the instability modes

Note from the formula (46) that the valve equilibrium position x_0 (obtainable by solving the equation (38)) is independent of the (dimensionless) pipe length parameter γ, whereas γ enters the right-hand side through $1/\omega_k^2 \propto (2k - 1)^2\gamma^2$. Hence we find that if a given valve is stable to the kth pipe mode according to the condition (46) then it will automatically be stable to the $(k + 1)$st mode also. In other words, if we think of pipe length γ as being a parameter, then the first mode to go unstable as we increase γ is the quarter wave ($k = 1$), followed by the 3/4-wave ($k = 2$), the 5/4-wave ($k = 3$) etc. Hence to find an instability threshold we only need to check the condition for the quarter-wave. The higher-order waves can only increase the number of unstable modes of an otherwise unstable situation.

This ordering argument applies only to linearised stability. In truth, simulations have shown that the limit cycle oscillations born at the quarter-wave Hopf bifurcation grow rapidly in amplitude and lead to fully nonlinear chatter (in which many pipe modes are excited) for pipe lengths that are significantly less than the higher pipe mode linear instability thresholds. See Section 4 below.

Another potential weakness of this argument is that we have ignored friction, convection and inlet pressure loss in this calculation. These effects are likely to become significant at higher mass flow rates. As we shall show in Section 5 below using numerical continuation, the ordering of the instability modes remains valid all the way up to flow rates at which the pipe flow becomes supersonic. In fact all instability curves come together to form a gross instability which kicks in at zero pipe length and Mach number equal to 1 (see the right-hand plot in Fig. 4 below). Note that to avoid such dramatic failure, capacity flow rates are designed so that the pipe flow remains subsonic ($M_{\mathrm{pipe}} = 0.44$ at $\dot{m}_{cap}$ for the JL2 valve on which we have based our parameters in this study).

3.3. Analytic approximation to quarter-wave instability threshold

Note from Table 2 that $\sigma\chi \ll 1$. So we shall make the further approximation that $\chi = 0$. Then it is further possible to simplify (45) for sufficiently small mass flow rates q by combining the stability criterion (38) with $k = 1$ and an approximation to the solution of the equation (38) in this limit. Note that for small $q \ll \sqrt{(\delta + 1)}$, we can seek an asymptotic expansion for x_0 in powers of q, from which we obtain

$$x_0 \approx \frac{q}{\mu\sigma\sqrt{1+\delta}} - \frac{q^2}{3\mu^2\sigma^2(1+\delta)^2} + \mathcal{O}(q^3). \tag{47}$$

Taking the first term in this expansion and substituting it into (46) we obtain

$$q > 2\frac{(1+\delta)^{3/2}}{\omega_1^2 - 1}\mu\sigma = 2\frac{4(1+\delta)^{3/2}\gamma^2}{\pi^2 - 4\gamma^2}\mu\sigma. \tag{48}$$

Note that equation (48) gives an asymptotic estimate for stability threshold as a function pipe length γ for small mass flow rates q and ignoring the inlet pressure loss χ (and the friction loss in the pipe ϕ). A more accurate expression can be obtained for higher flow rates and with inclusion of $\chi \neq 0$

21

by letting the solution to equation (38) be denoted $x_0(q)$, from which we obtain the more accurate implicit expression

$$(1 + \chi\sigma^2 x_0(q)^2)^2 x_0(q)^3 > 2q^2 \frac{4\gamma^2}{\pi^2 - 4\gamma^2} \frac{1}{\mu^2\sigma^2}. \tag{49}$$

In Sec. 5 below we shall compare both the explicit and implicit instability criteria against the exact computation of the Hopf bifurcation of the N-wave model. Both are found to provide good approximations, but, as expected the implicit formula is more accurate, especially for larger q values, see Fig. 6. The errors come about from the fact that the analytical criteria are derived under the assumption that $\chi = \phi = \Lambda = 0$.

4. Comparison with full model

All numerical investigations were carried using the dimensionless system of equations (13)–(15), (28), (29). But, for ease of practical interpretation, the results are presented in dimensional co-ordinates. All parameter values correspond to those in Tables 1 and 2 which are representative of a 2J3 valve. In what follows we shall refer to the the N-wave model (NWM) as the reduced model with N modes (i.e. equations (13)–(15) coupled to (28) and (29) with $k = 1, \ldots, N$) and the gas dynamical model (GDM) as the full system of equations as derived in Subsec. 2.1.

As an initial comparison, Fig. 2 presents valve lift time histories for two different mass flow rates — 20% and 70% of capacity — for a variety of pipe lengths. In each case we compare the results of the gas dynamic model (GDM, described in Section 2.1) with the NWM for $N = 1$ and $N = 3$, showing an initial transient for 0.1 seconds. The upper panel for each flow rate represents a case where the valve motion is stable. Note the close agreement between all three models in the case of the lower flow rate (left-hand plot). Analysis of the spectrum reveals that all the energy is in the quarter wave, with frequency ω_1, which for this flow rate is damped. For the higher flow rate (right-hand plot), there is agreement in the frequency of the damped oscillations (again ω_1), but the initial transient is larger (up to 95% of maximum valve) lift which causes significant quantitative difference between the GDM and the NWM for short times.

The middle panels show results in each case for a slightly longer pipe that is close to the instability threshold for that flow rate. Here again we see close
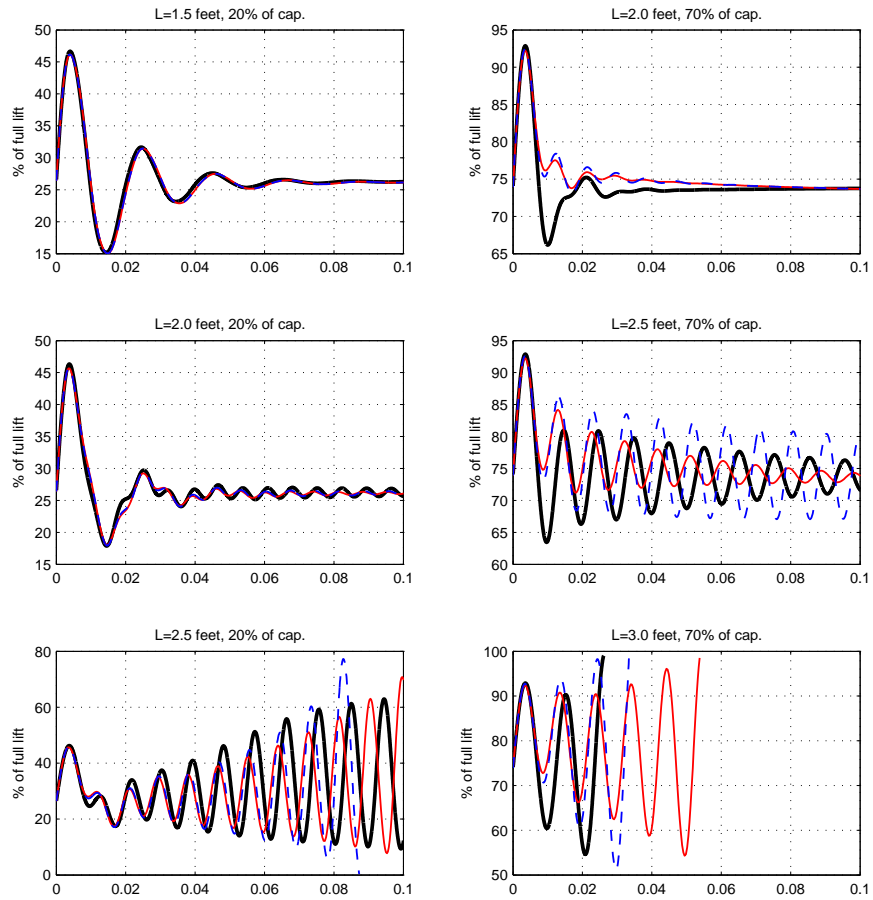
Figure 2: Comparison of the GDM (thick solid black line) and the NWM with 1 mode (thin solid red line) and three modes (thin dashed blue line). Colour version online.

agreement between the frequency and damping of the instability mode of the QWM and the NWM.

The lower panels of the figure show results for yet longer pipes which are beyond that for which valve flutter sets in. Here we see good initial comparison between the three models, but as the amplitude grows and the models start to depart as one would expect. In fact, if we continue the GDM for longer times we find the amplitude of oscillation grows in both cases until the valve contacts its seat (where lift = 0%). From then onwards chattering motion ensues. Recall that such contact is modelled as a hard impact, and so we see an impulsive reversal of the sign of valve velocity at each impact. Such an impact is likely to excite many higher-order pipe modes and so we should not expect good agreement between the NWM and GDM simulations for chattering motion.

Nevertheless, these results give confidence that the NWM is a good predictor of the point of instability and, for the dominant quarter-wave instability, $N = 1$ is sufficient to capture the instability. Note that to find such close quantitative as well as qualitative agreement for the case of the higher flow rate required correct evaluation of the constant χ measuring the degree of inlet pressure loss. Setting χ artificially to zero in the NWM resulted in appreciable differences with the GDM for both the equilibrium valve lift and the critical pipe length required for instability.

A clear advantage of the NWM is that it is much faster than the GDM. Each computational run in Fig. 2 took a fraction of a second for the NWM, compared with several minutes for the GDM (both implemented on a standard desktop computer). The real power of the NWM though is that it is possible to do parameter studies efficiently using numerical continuation. In particular, using this method we can trace precisely curves in two parameters at which Hopf bifurcations occur. For the GDM all we can do is simulate it at particular individual parameter values. In what follows, all numerical continuation results were performed using the software AUTO Doedel et al. (2007); Hegedus (2014).

Figure 3 shows the exact computation of the quarter-wave instability mode in the 3WM (three-wave mode, $k = 3$) compared with simulations of the full GDM. Note the agreement. This is to be expected since the stability threshold corresponds to where a pipe mode is first excited, with all other pipe modes being dormant. This is precisely the assumption that underlies the derivation of the NWM. What is more, we have repeated the computation of this instability curve using the NWM for different total numbers of modes
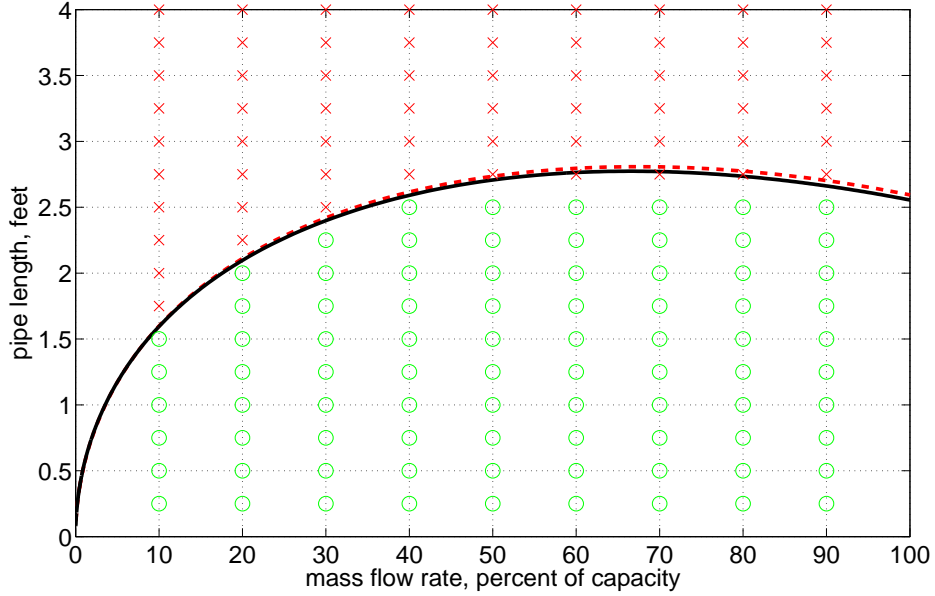
24

Figure 3: Stability map; critical pipe length as a function of mass flow rate. Crosses (red) indicated where the GDM simulations predict unstable behaviour, whereas (green) circles indicate where the simulations predict stability. The solid (black) line shows the stability boundary calculated by numerical continuation of the NWM for $N = 1$ (solid line) and $N = 3$ (dashed line, curves for $N = 4$ and $N = 5$ are indistinguishable from the $N = 3$ line). Colour version online.

N from 1 to 5. As expected from the way the NWM is derived, the instability curves computed this way are found to almost overlay each other (any small difference being due to the mild dependence of the coefficients a_1, b_1 etc on the total number of modes N).

It is worthwhile at this stage to comment on the structure of the instability curve in Fig. 3. Note the trend for low mass flow rates is there appears to be a near quadratic relationship between the minimum flow rate and the maximum pipe length for stability. As the mass flow rate increases, so the maximum stable pipe length also increases. However, for higher flow rates (beyond about 70% of capacity) this trend is reversed. If we were to run the valve beyond its rated capacity, then we find that at about 190% capacity, all
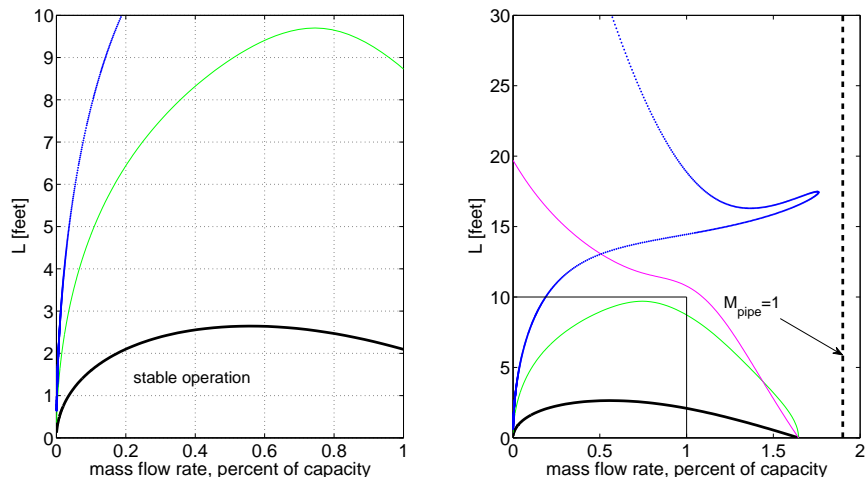
Figure 4: Hopf bifurcations of the pipe modes with of the 3-wave model. Solid thick black line: first (quarter-wave) Hopf bifurcation identical to the one shown in Figure 3. Thin solid lines: additional Hopf bifurcations, thick dashed vertical line: mass flow rate at which the pipe Mach number reaches 1.

pipe lengths lead to instability – see the extension of the solid black curve in Fig. 4 below. In fact, a careful calculation shows that the *pipe* Mach number is equal to one at just this flow rate, which can be seen by repeating the calculation after neglecting the inlet pressure loss term, i.e. setting $\chi = 0$. At this transition point any higher input mass flow rate becomes inconsistent. From the practical point of view, inlet pipe diameters are chosen in such a way that choked pipe flow cannot occur.

Figure 4 also shows loci of Hopf bifurcations corresponding to higher-order pipe modes. As predicted in Subsec. 3.3 we have found that these higher-order modes only go unstable for higher pipe lengths, which are already unstable to the quarter-wave mode. Indeed we see that the onset of the 1/4-wave, 3/4-wave and 5/4-wave pipe instability modes for small q scale as might be expected from the condition (46). That is, each instability scales approximately quadratically in the mass flow rate against pipe length, but with a quadratic coefficient that scales like $q^2/(\omega_k^2 - 1)$. That is, the q value for the instability of the kth-mode scales like $\sim 1/(2k - 1)$. This means that the higher-order pipe mode instabilities while potentially contributing to the complexity of the unstable dynamics, do not play a role in the onset

26

of instability and the stability region is bounded by the quarter-wave Hopf bifurcation curve alone.

5. Parameter studies

Having shown that only the quarter-wave Hopf bifurcation represents the threshold of stability, we shall now consider how this curve is affected by variation in various system parameters. All computations were carried out in AUTO using the 3WM unless otherwise stated.

5.1. Effect of set pressure

Note that the set pressure can be varied in our model by varying the dimensionless parameter δ which is proportional to the spring pre-compression. Figure 5 shows the effect on the instability curve of different set pressures. Note the clear trend that an increase in set pressure decreases the region of stability.

5.2. Comparison with analytic approximation

It is also instructive to see the effect that the friction and convective terms have on the shape of the instability curve. To that end the left-hand panel of Fig. 6 shows the same information as Fig. 5 with $p_{\text{set}} = 250\text{psi}$ but with each in term of Λ, ϕ and χ in (28) and (29) set to non-zero individually (the actual numbers are given in Table 2). We also show in this plot the analytical approximations (48) and (49) to this instability curve. It is interesting to note how well the implicit analytical formula (49) predicts the instability curve at least up to about capacity flow rate. We can also see that the inlet pressure loss χ, which is ignored in the simpler analytical formula (48). In contrast, pipe friction and convective terms have a much smaller effect.

5.3. Effect of other valve properties

In principle, using numerical continuation, we can also vary other dimensionless parameters appearing in the model. These mostly affect properties of the pipe geometry and fluid properties. Since this study is limited to valve characteristics we have not presented the details here. We do note the general trend though that the dimensionless parameter β is crucial. If β is $\mathcal{O}(1)$ or greater as would be the case for liquids, we find very different results (as for example the case studied in Bazsó et al. (2014a)).
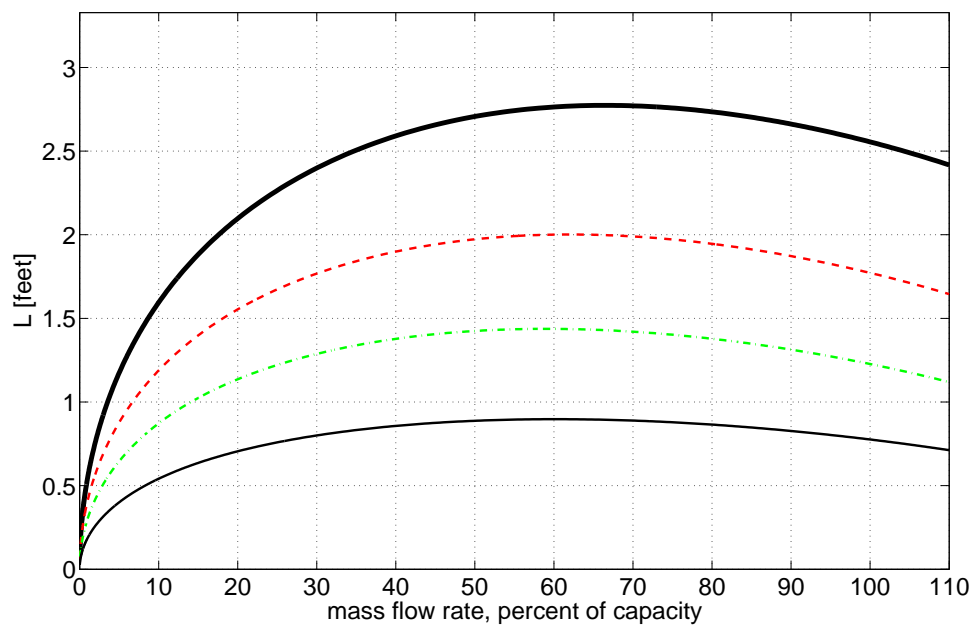
Figure 5: Effect of set pressure (from top to bottom): 250 psi (thick black solid line), 500 psi (thin red dashed line), 1000 psi (this green dash-dot line), 2500 psi (solid black line). Colour version online.
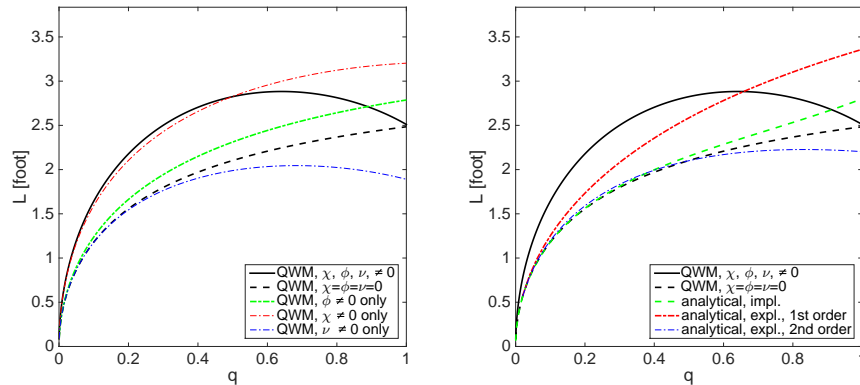
28

Figure 6: (Left panel) Effect of inlet pressure drop χ, pipe friction ϕ and the convective terms ν on the stability boundary, see text for details. (Right panel) Comparison between the simple analytical prediction (48) (red dash-dot line), the more accurate implicit formula (49) (blue dash-dot line) and the second-order approximation, i.e. combining (47) with (49) and the true instability curve (solid and dashed black line) of the quarter-wave model using AUTO. Dimensionless parameter values are as in Table 2. Colour version online.

The results so far have been computed with the valve damping set to zero. This is not necessarily unrealistic, because design codes specify that the valve should open unimpeded. Also, in practice any viscous damping in the valve spring is likely to be much weaker than the damping (either positive or negative) due to fluid effects.

The estimation of damping parameters in lightly-damped mechanical system is not typically an easy task. Nevertheless, we have recomputed the stability curve in the presence of different for different values of the valve damping. Fig. 7 shows the results for 1%, 10%, and 100% of critical damping. As expected, inclusion of damping is in a general stabilizing effect, but this is only appreciable in the case of valves that are critically (100%) or damped or higher.

We have also tried variation of reservoir volume and found that halving this volume, doubling it, or multiplying it by a factor ten makes no appreciable difference to the instability curve whatsoever. This is to be expected because reservoir volume affects only the parameter β, which as explained in Subsec. 3.3 is very much less than $O(1)$ and does not enter into the instability prediction analysis. Increasing the reservoir volume only makes β smaller.
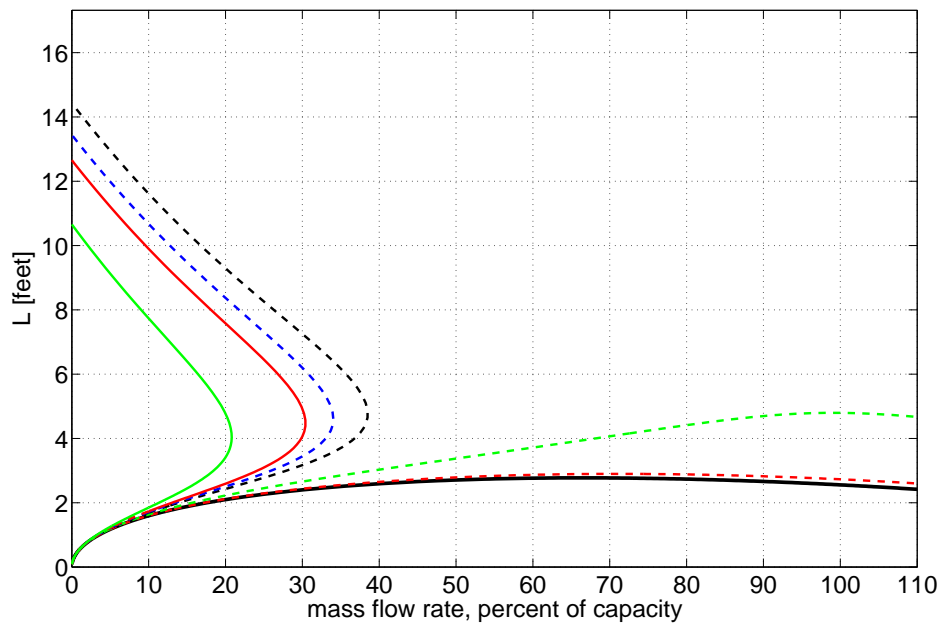
29

Figure 7: Effect of viscous valve damping. From bottom to top: 0, 10, 50, 90, 100, 110 and 150 percent of critical damping $k_{crit} = 2\sqrt{sm}$.

6. Summary and outlook

In summary, this paper has extended the earlier analysis in Hős et al. (2014) by deriving a generalized low-order model of a direct spring-loaded pressure relief valve connected to a reservoir via a straight pipe of the same diameter as the valve inlet flange. In that earlier work we were able to show the agreement between the onset of instability in experimental tests on three different valves and full gas dynamical simulation model. This work in contrast has been all about explaining the origins of that instability and providing a realistic tool for conducting parameter studies. For that purpose we have deliberately presented no new experimental evidence.

The so-called NWM we have derived, enabled us in Sec. 3 to analyse several different possible modes of instability and to argue that only the instability associated with the lowest-order pipe mode, the so-called quarter-wave instability is likely to be of significance for valves in gas service. As shown in Sec. 3.3, this mode comes about because the valve effectively provides negative damping to the pipe mode for sufficiently long pipes or slow flow rates. Another consequence of this finding is that the instability is perfectly predictable from a simple 1-mode truncation. That is, the simple quarter-wave model, as first derived in Bazsó et al. (2014b) can be used as a predictive tool.

Moreover, we have provided a simple analytical criterion for predicting the instability threshold, Equation (48), and its more accurate implicit form (49). This is found to be a good predictor of the general shape of the instability curve for the experimental parameter values used in this study, and to be exact in the limit of low mass flow rates and low inlet pressure drop. The efficacy of this analytical approximation in practice for other valve and pipe geometries will be left for future work.

The main purpose of our reduced-order modelling has been to enable simple parametric studies. The reduction to a low-dimensional dimensionless system of equations enables us to apply numerical continuation to delineate the onset of the instability in parameter space even up to capacity flow rates, for a wide range of different valves and configurations. From the preliminary parametric studies in Sec. 4 several conclusions can be drawn. First, increase of set pressure has a general destabilizing effect. Moreover, although pipe friction can have a stabilizing effect for long pipes or high mass flow rates, this is over-ridden by the destabilizing effect of fluid convection at high flow rates. Also, to get close quantitative agreement with the full gas-dynamic

31

simulations, we need to treat the inlet pressure loss carefully.

We have found that the instability cannot fundamentally be avoided simply by varying valve parameters. Nevertheless, decreasing set pressure and valve damping all have a positive effect on the stability region. The most interesting case is that of valve damping. As shown in Fig. 7 taking realistic damping of 10% of critical or less, has little or no quantifiable effect on the stability region. Only damping values close to critical damping can greatly alleviate the instability, and for significant flow rates make it disappear altogether. However, such a large viscous damper in parallel with the valve spring would run counter to current design codes which require the valve to open unimpeded.

We have also found that running the valve near its stated capacity can increase instability (owing to fluid convection - high Mach number - effects). The effective Mach number in the pipe seems to be a key quantity; if the flow is close to supercritical in the pipe we find that the stability region is greatly reduced, with no stability at all being possible as Mach number approaches unity.

Only tentative conclusions can be drawn from these results about possible remedies to avoid the instability in practice. We should also stress that there are many parameters in the problem (see Table 2), despite our attempts to reduce them to a list of dimensionless groupings. We have not done an exhaustive search of parameters relating to fluid properties such as σ, α and β. Having said this, it seems clear that pipe pressure loss is not the primary mechanism behind valve chatter. Thus trying to reduce the frictional pipe loss (as in the API standard RP520 'three percent rule', see Hős et al. (2014)) will not make this fundamental quarter-wave instability go away.

There are many avenues of research that remain to be investigated. For example, the effect of back pressure, an analysis of other valve topologies such as pilot-operated valves and a better understanding in practice of the interplay between different instability modes in liquids. These will all form the subject of future work.

Acknowledgements

References

Bazsó, C., Champneys, A., Hős, C., 2014a. Bifurcation analysis of a simplified model or a pressure relief valve attached to a pipe. To appear in *SIAM J. Applied Dynamical Systems*.

Bazsó, C., Champneys, A., Hős, C., 2014b. Model reduction of a direct spring-loaded pressure relief valve with upstream pipe. To appear in *IMA J. Applied Math*.

Botros, K., Dunn, G., Hrycyk, J., 1997. Riser-relief valve dynamic interactions. Journal of Fluids Engineering 119, 671–679.

Canuto, C., Hussaini, M., Quarteroni, A., Zang, T., 2007. Spectral Methods: Evolution to Complex Geometries and Applications to Fluid Dynamics. Springer, New York.

Doedel, E., Champneys, A., Fairgrieve, T., Kuznetsov, Y.A., Sandstede, B., Wang, X., 2007. Auto07p, continuation and bifurcation software for ordinary differential equations (with homcont). Available at `http://sourceforge.net/projects/auto-07p/` (accessed 24/06/2014).

Hayashi, S., 1995. Instability of poppet valve circuit. JSME International Journal. Ser. C, Dynamics, Control, Robotics, Design and Manufacturing 38, 357–366.

Hegedus, F., 2014. Stable bubble oscillations beyond Blake's critical threshold. ULTRASONICS 54, 1113–1121. doi:10.1016/j.ultras.2014.01.006.

Hős, C., Champneys, A., Paul, K., McNeely, M., 2014. Dynamic behaviour of direct spring loaded pressure relief valves in gas service: model development, measurements and instability mechanisms. Submitted to the *Journal of Loss Prevention in the Process Industries*.

Izuchi, H., 2010. Stability analysis of safety valve. American Institute of Chemical Engineers, *10th Topical Conference on Natural Gas Uitilization ISBN: 9781617384417*.

Kuznetsov, Y., 2004. Elements of applied bifurcation theory. Springer-Verlag.

Zucker, D., Biblarz, O., 2002. Fundamentals of Gas Dynamics. New York: John Wiley and Sons.